Matrix–Guest Energy Transfer in Matrix-assisted Laser Desorption†

Akos Bencsura[1], Vivek Navale[2], Mehrnoosh Sadeghi[2] and Akos Vertes[2]*
[1]Department of Chemistry, Catholic University of America, Washington D.C. 20064, USA
[2]Department of Chemistry, George Washington University, Washington D.C. 20052, USA

Molecular dynamics was used to analzye energy transfer rates between matrix and guest molecules in matrix-assisted laser desorption allowing for a large number of internal degrees of freedom. The effect of initial matrix temperature jump on internal energy equilibration times and on guest limiting temperatures has been studied on a model system comprising a pyridine-3-carboxylic acid matrix and leucine enkephalin (Tyr-Gly-Gly-Phe-Leu) guest molecule. It appears that the energy transfer rates between matrix and guest molecules depend on the initial matrix temperature jump. The initial matrix temperature of 900 K leads to incomplete desorption, whereas at 1500 K complete desorption and the formation of an energy-transfer bottleneck was observed. Following the guest center-of-mass at different initial matrix temperatures indicates that in the case of 1500 K and 3000 K the desorption process is complete, whereas at 900 K the guest molecule stays near the matrix surface. In the case of complete desorption deeper embedding of the guest molecules leads to somewhat lower guest limiting temperatures. Uniformly higher limiting temperatures are observed for higher laser irradiance and the increase in burial depth leads to more complete equilibration between the two species. © 1997 by John Wiley & Sons, Ltd.

The advent of the matrix assisted laser desorption/ionization (MALDI) method in combination with mass spectrometry has led to a valuable means of macromolecular mass measurement. A variety of biological molecules: proteins, carbohydrates, nucleotides and synthetic polymers have been characterized by the application of the MALDI-MS method.[1] Currently, the method is being applied towards sequencing of nucleotides,[2] an effort which could ultimately lead to the rapid means of profiling genomes of various organisms.[3]

Despite these impressive strides in MALDI applications, the understanding of the fundamental processes involved during and after the interaction of laser light and sample is far from being complete. More specifically, the mechanism of volatilization and ionization has not been clearly understood. The choice of matrix and desorption conditions such as laser irradiance has been shown to result in different degrees of fragmentation. In addition, the observation of fragmentation processes is known to be related to the time-scale of the mass analysis.[4] It is also apparent that the low sublimation temperature of the matrix, the sub-critical concentration of the guest molecules, and the rapid laser energy deposition (compared to the sublimation induction period) influence the yield of high-mass particles.[5] In the light of these observations, the homogeneous bottleneck (HB) model for the MALDI process has earlier been proposed.[6,7]

Briefly, the model is homogeneous in the sense that the energy is assumed to be uniformly deposited into the internal degrees of the matrix within the interaction volume. In ultraviolet (UV) MALDI this process involves electronic excitation of the matrix followed by internal conversion leading to highly excited vibrational states within the first few ps of illumination. Infrared (IR) MALDI is believed to start with energy deposition into certain vibrational degrees of freedom of the matrix. For example, the Er:YAG laser irradiation of a succinic acid matrix at 2.94 µm leads to the excitation of the O–H stretching modes. Thus, in both UV and IR MALDI a strongly nonequilibrium situation develops, whereby most of the deposited energy is concentrated in the vibrational modes of the matrix. There are two competing processes during energy redistribution: (a) energy transfer from the matrix to the guest molecules, and (b) desorption induced by sublimation. According to the HB model the internal energy of the guest molecules lags behind that of the matrix due to a bottleneck in the transfer of energy between the matrix and guest molecules. The *ad hoc* assumption of this bottleneck, however, could not be justified within the framework of a phenomenological kinetic model.

The molecular dynamics (MD) method compared to the phenomenological models reviewed earlier,[8] has the advantage of being able to account for the internal structure of matrix and guest molecules. Several of the MD codes are being used to describe conformational changes of macromolecules in an environment of small molecules.[9] In these MD descriptions only the fragmentation of the matrix and the ionization processes are neglected.

Previous computational studies of laser desorption were limited to systems with no[10] or with only a few internal degrees of freedom.[11] Obviously, a protein embedded in a complex organic matrix does not fall into any of these categories. Thus, the present work attempts to describe the evolution of energy transfer between the internal degrees of freedom of complex matrix and guest molecules using MD simulations. Investigating the effect of different laser irradiances and guest burial depths at a molecular level yields

results that can be compared to experimental data. Our objective is to enhance the microscopic understanding of co-evaporation and energy equilibration during the MALDI process.

METHODS OF CALCULATION

The methods used in these calculations are similar to the ones described in our earlier publication.[12] Briefly, in order to model the host–guest interaction in the embedding process and the crystal dynamics upon laser excitation, we applied an MD code that had been developed to describe protein and nucleic acid behavior in an aqueous environment. The chemistry at Harvard molecular mechanics (CHARMM)[13] code relies on the atom- and group-based treatment of nonbonded interactions between the macromolecule and its molecular environment. In order to simplify the model, both ionization and fragmentation of the molecules are neglected, thereby reducing the number of interactions during modeling.

A leucine enkephalin (Tyr-Gly-Gly-Phe-Leu) guest molecule and the surrounding pyridine-3-carboxylic acid (nicotinic acid) matrix were represented by their detailed molecular structures. The CHARMM (Versions c22g5, c23f4, and c24b2) MD simulations were carried out by specifying a crystalline non-aqueous medium (matrix) and by introducing an initial matrix temperature jump (representing laser heating of the matrix) that led to a phase transition. During the simulations, only polar hydrogen atoms were incorporated explicitly; nonpolar groups were modeled as extended atoms. Also, the empirical potential energy function consisted of bond stretching, bending, dihedral, improper, Coulomb, and van der Waals energy terms. The forces stemming from the non-bonding interactions were smoothly switched to zero between 800 and 1200 pm.[14] The potential energy parameters for the amino acid residues and, in part, for the nicotinic acid were taken from the standard parameter file of the CHARMM program. Missing parameters for the nicotinic acid were estimated by using quantum chemical calculations. Wave functions and charge distributions of the nicotinic acid molecule were calculated using the GAMESS *ab initio* program for the fully optimized structure at the 3-21G* level.[15] The CHelpG feature of the GAMESS program provided the electrostatic-potential-derived atomic charge distributions.[16]

The desorption simulations were carried out by applying a stochastic boundary molecular dynamics method.[17] In order to simplify and accelerate the MD calculations of the solid–vacuum interface, hemispherical boundary conditions were used. For that purpose, using the X-ray based crystallographic structure, a hemisphere of the nicotinic acid matrix was constructed with a maximum diameter of 4800 pm.[18] The initial matrix coordinates were established by repeating the unit cell six times in all three axis directions (x, y and z). A hemisphere with 2300 pm average radius containing 202 nicotinic molecules was outlined by deleting all the molecules with $y > 0$ within a sphere with a radius of 2200 pm.[12] The structure was energy minimized and a fully extended leucine enkephalin molecule was incorporated into the matrix. The backbone of the peptide was aligned parallel to the rings of the nicotinic acid

matrix, and the center-of-mass of the peptide molecule was at –280 pm for shallow embedding and at –1050 pm for deep embedding. The stretched conformation, parallel alignment, and the burial depths of the peptide were selected arbitrarily since no data on peptide behaviour in a nicotinic acid environment were available. Trial runs with different conformations and different alignments, however, convinced us that these two factors had little effect on the processes of our interest. In preparation for the dynamics simulation the entire structure was energy minimized again using the Newton–Raphson method.

The hemispherical volume was delineated into three regions: the reaction region containing all atoms within a 1900 pm radius sphere, atoms between 1900 and 2200 pm made up the buffer region and beyond 2200 pm was the reservoir region. Both the reaction region and the flat face of the hemisphere were unrestrained throughout the simulation. However, the movement of the atoms in the buffer and reservoir regions were restrained by a 0.084 kJ/mol × pm harmonic force. Also, a uniform 200 ps^{-1} frictional coefficient was employed on all heavy atoms in the buffer region. The dynamics equations of motions were numerically integrated with the leap-frog integrator using 1 fs time step.[12]

Four different initial matrix temperature values (900, 1200, 1500 and 3000 K) were used to represent the variation of laser power densities. The effect of burial depth was investigated using the shallow (280 pm) and deep (1050 pm) embedding situations as examples. At first, however, room temperature equilibration was carried out at a temperature of 300 K for a period of 45 ps. Subsequently, the initial temperature of 300 K was suddenly increased to the higher temperatures (levels indicated above) by instantaneously scaling the velocities of the atoms in nicotinic acid, and thereby simulating the laser excitation process.

A cluster of Indigo, Indigo^2, and Indy workstations (Silicon Graphics, Mountain View, CA, USA) was used to perform the MD calculations and to analyze the results. The coordinates and velocities of all particles were saved in 100-step increments for analysis and the trajectories were visualized and animated by the
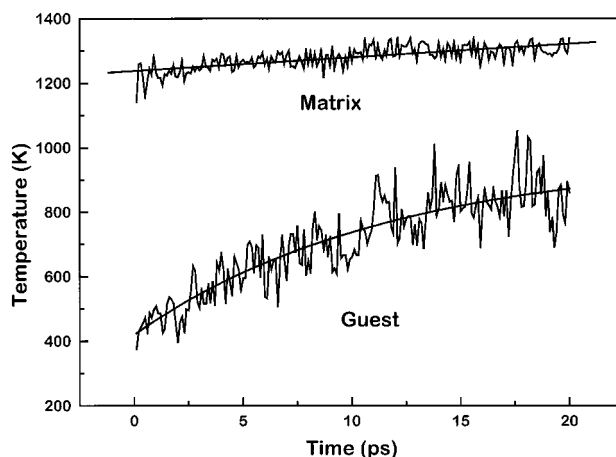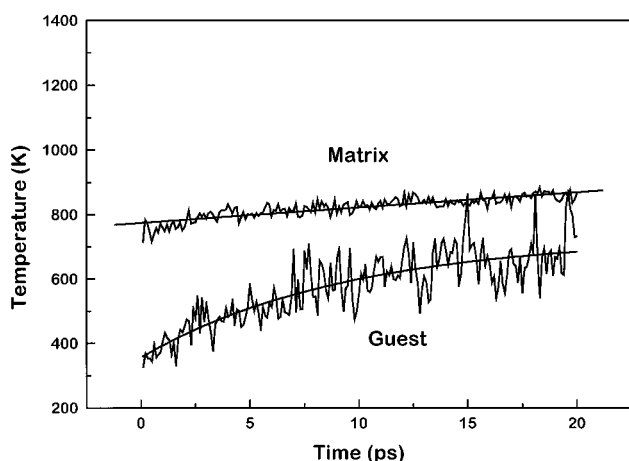

Figure 1. Evolution of matrix–guest molecule internal temperatures at adiabatic initial matrix temperature jump to 1500 K (for shallow embedding).

SCARECROW package (Center for Scientific Computing, Espoo, Finland).

RESULTS AND DISCUSSION

In order to study the energy transfer between matrix and guest molecules, it was necessary to differentiate their temperature histories after the matrix excitation. Initial matrix temperatures of 900 K, 1200 K, 1500 K and 3000 K have been examined. It appears that the energy transfer rates between matrix and guest molecules depend on the initial matrix temperature jump. Examining the trajectories in the 20 ps time domain made it clear that we had to differentiate between incomplete (900 K) and complete (1500 K and 3000 K) desorption. The desorption at 1200 K showed intermediate characteristics between these two limiting cases. In our view longer calculation times would be necessary to classify the 1200 K case into the desorption or no-desorption categories.

The matrix and guest temperature profiles with an instantaneous initial temperature of 1500 K are presented in Fig. 1. It is evident that while the temperature of the matrix reaches 1300 K, the temperature of the guest molecules stays significantly lower. The prediction
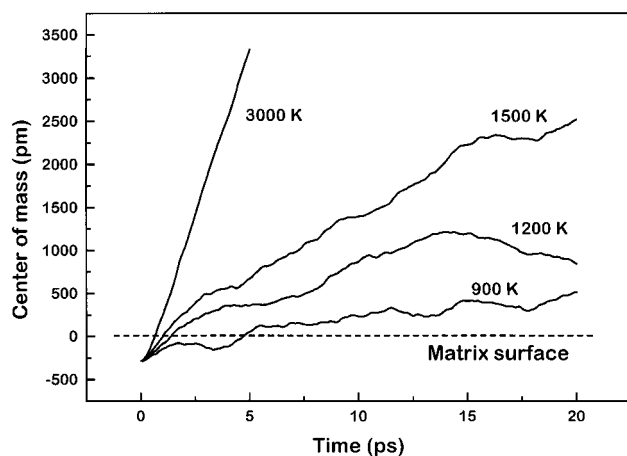
Table 1. Comparison of limiting temperatures, T_{lim}, and relaxation times, τ, of the guest molecules for two different guest burial depths and two different initial matrix temperatures.

Burial Depth:	Shallow (280 pm)		Deep (1050 pm)	
	900K	1500K	900K	1500K
T_{lim} (K)	738	973	874	875
τ (ps)	9.7	12	14	14

of the HB model seems to prevail in this case. The internal temperature of the guest molecules increases with a relaxation time of 12 ps to ~ 973 K, a value substantially lower than the matrix temperature. Although the desorption process (crossing the matrix surface) takes place at ~ 550 K, further collisions in the dense region of the plume lead to an additional increase in the guest temperature.

In Fig. 2. the matrix and guest molecule temperature histories are shown for an initial matrix temperature of 900 K (incomplete desorption). The results indicate that at a lower initial matrix temperature, corresponding to a lower laser irradiance, the temperature of the guest molecules approaches the matrix temperature more rapidly (time constant of 9.7 ps with a limiting temperature of about 738 K). This observation is consistent with the notion that the migration of the guest molecule to the surface is slower in this case; thereby it spends more time in the dense condensed phase and undergoes more collisions. Even though the guest molecule does not depart from the matrix surface during the observation period, we call this case incomplete desorption because the laser heating leads to the segregation of the matrix–guest system. This effect can be rationalized by the energetically unfavored initial position of the guest molecule inside the matrix crystal. Although incomplete desorption leads to better temperature equilibration between matrix and guest particles, the corresponding lower matrix temperatures mean lower limiting temperatures for the guest molecules. Thus, the lack of energy transfer bottleneck in this case does not lead to guest fragmentation.

These observations are complemented by tracking the center-of-mass of the guest molecule at different matrix temperatures (Fig. 3). In the case of 1500 K and

Figure 2. Temperature history of the matrix and shallowly buried guest molecules at an instantaneous jump to initial 900 K matrix temperature.

Figure 3. Leucine enkephalin center-of-mass position as a function of time for different matrix temperature changes corresponding to varying laser irradiances.
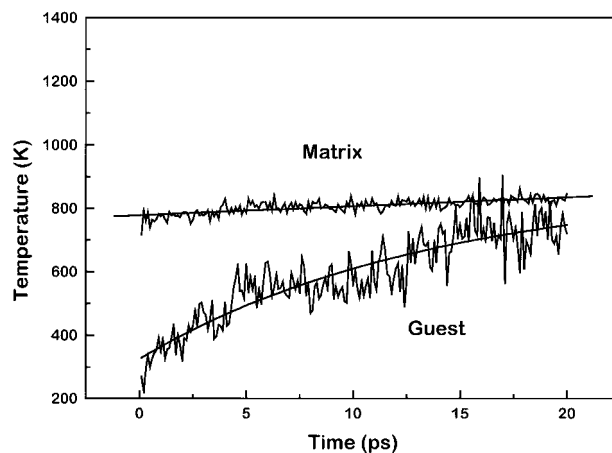
Figure 4. Temperature profiles for deep embedding of the guest molecules after a jump to 900 K initial matrix temperature.

3000 K matrix temperatures, the guest molecule desorption process is clearly complete. However, at 900 K the guest molecule seems to be stalled near the matrix surface. These results are coherent with the experimental observation of threshold irradiance and the influence of the laser irradiance on the fragmentation process in MALDI.[1]

Furthermore, we investigated the effect of the burial depth of guest molecules in the matrix. These calculations indicate that in the case of complete desorption (1500 K) the deeper embedding of the guest molecules in the matrix crystal leads to somewhat lower guest molecule temperatures. Comparison of the limiting temperatures and relaxation times at shallow and deep embedding is shown in Table 1. Uniformly higher limiting temperatures are observed for higher laser irradiance. The comparison of Figs 2 and 4 indicate the effect of guest burial depth on the energy redistribution process for incomplete desorption (900 K). In contrast to Fig. 2, Fig. 4 depicts the temporal behavior of matrix and guest internal temperatures for a deeply embedded guest molecule. The increase in burial depth leads to a more-complete equilibration between the two species. This effect can be rationalized by the longer trajectory and the larger number of collisions it takes for the guest molecules to reach the surface, starting from a deeper location.

Acknowledgements

REFERENCES

1. F. Hillenkamp, M. Karas, R. Beavis and B. T. Chait, *Anal. Chem.* **63**, 1193A (1991).
2. G. Talbot and M. Mann, *Rapid Commun. Mass Spectrom.* **10**, 100 (1996).
3. G. Hurst, M. J. Doktycz, A. A. Vass and M. Buchanan, *Rapid Commun. Mass Spectrom.* **10**, 377 (1996).
4. Q. Jun, R. J. Steenvorden and B. T. Chait, *Proceedings of the 42nd Annual Conference on Mass Spectrometry and Allied Topics*, Chicago, IL ASMS, Santa Fe, 1994, p. 5.
5. A. Vertes, G. Irinyi and R. Gijbels, *Anal. Chem.* **65**, 2389 (1993).
6. A. Vertes, R. Gijbels and R. D. Levine, *Rapid Commun. Mass Spectrom.* **4**, 228 (1990).
7. A. Vertes and R. D. Levine, *Chem. Phys. Lett.* **171**, 284 (1990).
8. R. E. Johnson, *Int. J. Mass Spectrom. Ion Processes* **139**, 25 (1994).
9. K. B. Lipkowitz and D. B. Boyd, *Reviews in Computational Chemistry* **6**, Appendix 2, VCH, Weinheim (1995).
10. J. Shiea and J. Sunner, in *Methods and Mechanisms for Producing Ions from Large Molecules* K. G. Standing and W. Ens (Eds). Plenum Press, New York (1991) p. 147.
11. T. A. Holme and R. D. Levine, *Surf. Sci.* **216**, 587 (1989).
12. A. Bencsura and A. Vertes, *Chem. Phys. Lett.* **247**, 142 (1995).
13. B. R. Brooks, R. E. Bruccoleri, B. D. Olafson, D. J. States, S. Swaminthan and M. Karplus, *J. Comput. Chem.* **4**, 187 (1983).
14. P. J. Steinbach and B. R. Brooks, *J. Comput. Chem.* **15**, 667 (1994).
15. M. W. Schmidt, K. K. Baldridge, J. A. Boatz, S. T. Elbert, M. S. Gordon, J. J. Jensen, S. Koseki, N. Matsunaga, K. A. Nguyen, S. Su. T. L. Windus, M. Dupuis and J. A. Montgomery, *J. Comput. Chem.* **14**, 1347 (1993).
16. C. M. Breneman and K. B. Wiberg, *J. Comput. Chem.* **11**, 361 (1990).
17. A. Brunger, C. L. Brooks III and M. Karplus, *Proc. Natl. Acad. Sci. US* **82**, 8458 (1985).
18. W. B. Wright and G. S. D. King, *Acta Cryst.* **6**, 305 (1953).